

# Violation of chirality of the Möbius domain-wall Dirac operator from the eigenmodes

Guido Cossu\*

*Theory Center, IPNS,  
High Energy Accelerator Research Organization (KEK),  
Tsukuba, Ibaraki 305-0810, Japan*

Hidenori Fukaya<sup>†</sup> and Akio Tomiya<sup>‡</sup>

*Department of Physics, Graduate School of Science,  
Osaka University, Toyonaka, Osaka 560-0043, Japan*

Shoji Hashimoto<sup>§</sup>

*Theory Center, IPNS, High Energy Accelerator Research Organization (KEK),  
Tsukuba, Ibaraki 305-0810, Japan and  
School of High Energy Accelerator Science,  
The Graduate University for Advanced Studies (Sokendai), Tsukuba 305-0801, Japan*

## Abstract

We investigate the effects of the violation of the Ginsparg-Wilson (GW) relation in the Möbius domain-wall fermion formulation on the lattice with finite fifth dimension. Using a decomposition in terms of the eigenmodes of its four-dimensional effective Dirac operator, we isolate the GW-violating terms for various physical quantities including the residual mass and the meson susceptibilities relevant for the effective restoration of the axial U(1) symmetry at finite temperature. Numerical result shows that the GW-violating effect is more significant, or even overwhelming, for the quantities that are dominated by the low-lying eigenmodes.

PACS numbers: 11.15.Ha, 11.30.Rd

---

\* cossu@post.kek.jp

† hfukaya@het.phys.sci.osaka-u.ac.jp

‡ akio@het.phys.sci.osaka-u.ac.jp

§ shoji.hashimoto@kek.jp

## I. INTRODUCTION

Chiral symmetry is a notable property of the QCD lagrangian. Its spontaneous breaking induces significant phenomenological properties of low-energy QCD as described by chiral effective theories. In the lattice study of low-energy QCD it is therefore highly desirable to maintain the chiral symmetry on the lattice to have cleaner control of the chiral properties. Indeed, there is a class of physical quantities that are sensitive even to tiny violations of chiral symmetry. A well-known example is the difference between vector and axial-vector vacuum polarization functions  $(\Pi_{VV} - \Pi_{AA})(Q^2)$ , which vanishes in the limit of unbroken chiral symmetry. In its numerical study on the lattice [1] chiral symmetry plays a crucial role. Another important example is the difference of the meson susceptibilities  $\chi_\pi - \chi_\delta$ , which is an order parameter of the flavor-singlet axial  $U(1)$  symmetry and it is used in the study of effective restoration of axial  $U(1)$  at finite temperature (for recent lattice studies see [2–5]). Written in terms of fermion eigenmodes, it is a weighted average of the Dirac eigenvalue spectrum  $\rho(\lambda)$  with the dominant contribution from the lowest end of the spectrum, and thus any small effect of chiral symmetry violation on the near-zero Dirac eigenmodes may substantially affect the result.

In this work we study the effect of the violation of chiral symmetry on the lattice with an application to the meson susceptibilities in mind. We consider a variant of the domain-wall fermion formulation [6–8], which realizes chiral symmetry on the lattice very precisely but not exactly, and formulate the remnant violation of chiral symmetry in the basis of the Dirac eigenmodes. Then, we are able to identify and monitor the violation for each eigenmode and to trace its effect on the physical quantities such as the meson susceptibilities. In addition to the meson susceptibilities, we also analyze the residual mass and the chiral condensate as simpler examples.

We use the lattice ensembles generated for a study of finite temperature phase transition with the Möbius domain-wall fermion. The physical results will be presented in a separate paper.

The paper is organized as follows. In Section II we first review the lattice fermion formulation that we use in this study and then decompose the meson susceptibilities and other quantities in the Dirac eigenmodes basis in Section III. In Section IV we show that at finite temperature the contribution of the GW violation to the susceptibilities on coarse lattices

may dominate the signal. We repeat the same analysis for  $m_{\text{res}}$  and show mode by mode which are the major contributions of the GW violation term to the residual mass. We then summarize our results.

## II. CHIRAL SYMMETRY ON THE LATTICE

### A. Möbius domain-wall fermion

Designing a discretized Dirac operator  $D$  that preserves chiral symmetry without introducing unwanted doublers had been a long standing problem in lattice field theory before the domain-wall [6–8] and overlap fermions [9, 10] were discovered. Doublers inevitably appear on the lattice if we insist on the continuum anti-commutation relation  $\{\gamma_5, D\} = 0$  for the lattice Dirac operator with the generator of the chirality transformation  $\gamma_5$ . This is known as the no-go theorem by Nielsen-Ninomiya [11]. The solution to this conundrum was to modify the anti-commutator as

$$\{\gamma_5, D\} = aRD\gamma_5D, \quad (2.1)$$

which is called the Ginsparg-Wilson (GW) relation [12].  $R$  could be any local operator that commutes with  $D^\dagger D$ . Any operator satisfying this relation has an exact chiral symmetry at finite lattice spacing  $a$  [13]. For a constant  $R$ , which we take  $R = 2$ , a formal solution is known, *i.e.* the overlap Dirac operator [9, 10]:

$$D_{\text{ov}} = \frac{1}{2} [1 + \gamma_5 \text{sgn}[H_K(M_5)]], \quad (2.2)$$

where the kernel  $H_K$  is an hermitian Wilson-like operator  $\gamma_5(D_K - M_5)$  with a large negative mass term  $M_5$ . Here and in the following we omit the lattice spacing for simplicity; physical quantities are to be extracted after multiplying an appropriate factor of  $a$ .  $D_{\text{ov}}$  has all desirable properties of a chirally symmetric operator at the cost of evaluating the matrix sign function, which is possible but the lattice size that could be treated with a given machine time is much more limited than with other (non-chiral) lattice fermion formulations. For attempts of its large-scale simulation see for instance [14, 15]. A closely related formulation is the so-called domain-wall fermion [6–8]. By introducing a five-dimensional (5D) fermionic field with special boundary conditions, it realises a chiral fermion mode on its four-dimensional

(4D) boundaries. An equivalence of the two formulations can be proved explicitly in the limit of large fifth dimension  $L_s \rightarrow \infty$  [16–19].

There are related lattice fermion formulations of the domain-wall class other than its original form [8]. They have different structures of 5D Dirac operators, generally written as  $D_{\text{DW}}^{5d}(m)$ ; after constructing the 4D effective Dirac operator they are distinguished by the form of the kernel operator  $H_K$  and the sign function approximation. The 4D effective Dirac operator is constructed as

$$D_{\text{DW}}^{4d}(m) = [\mathcal{P}^{-1}(D_{\text{DW}}^{5d}(1))^{-1}D_{\text{DW}}^{5d}(m)\mathcal{P}]_{11}, \quad (2.3)$$

where  $\mathcal{P}$  is a permutation matrix defined in the 5D space to place the left-handed and right-handed modes of the physical 4D field on the opposite 4D surfaces of the 5D space.  $D_{\text{DW}}^{5d}(1)$  is the Pauli-Villars regulator to kill unnecessary degrees of freedom in the 5D space. For the simple cases that the structure of the 5D operator does not depend on the coordinate  $s$  of the fifth direction, the form of the 4D effective operator is given as

$$D_{\text{DW}}^{4d}(m) = \frac{1+m}{2} + \frac{1-m}{2}\gamma_5 \frac{T(H_K)^{-L_s} - 1}{T(H_K)^{-L_s} + 1}, \quad (2.4)$$

with  $T(H_K) = (1 - H_K)(1 + H_K)^{-1}$ .

In the so-called Möbius domain-wall fermion [20] the kernel is given by

$$H_K(M_5) = \gamma_5 \frac{(b+c)D_W(M_5)}{2 + (b-c)D_W(M_5)}, \quad (2.5)$$

where  $D_W$  is the standard Wilson-Dirac operator defined on four-dimensional slices of the five-dimensional space. Two parameters  $b$  and  $c$  can be adjusted to control the chirality properties. It includes two common choices as special cases: (i)  $b+c=2$ ,  $b-c=0$ , the Borici kernel [21], and (ii)  $b+c=b-c=1$ , the Shamir kernel [7]. One can also use a different setup  $b+c=\alpha$ ,  $b-c=1$ , which is called the scaled-Shamir kernel [20]. The scale factor  $\alpha$  is to be chosen such that the sign function approximation is optimized [20].

At any finite  $L_s$ , the 4D effective operator  $D_{\text{DW}}^{4d}(0)$  slightly violates the GW relation. By writing

$$\{\gamma_5, D_{\text{DW}}^{4d}(0)\} - 2D_{\text{DW}}^{4d}(0)\gamma_5 D_{\text{DW}}^{4d}(0) = \gamma_5 \Delta, \quad (2.6)$$

$\Delta$  expresses the defect in the approximation of the sign function

$$\Delta = \frac{1}{4} (1 - \text{sgn}^2(H_K)). \quad (2.7)$$

The effect of this small violation of chiral symmetry can be written in terms of matrix elements of relevant operators including  $\Delta$ . In the next section we consider such matrix elements in the space spanned by the eigenmodes of hermitian operator  $H_m \equiv \gamma_5 D_{\text{DW}}^{4d}(m)$ . Their contributions to the physical quantities, such as the meson susceptibilities and chiral condensate, are then studied quantitatively on finite temperature lattices.

## B. Residual mass

The residual mass  $m_{\text{res}}$  is a standard estimate of the GW violation in the domain-wall fermion formulation. It represents the additive renormalization to the quark mass from the remnant violation of chiral symmetry at finite  $L_s$ . Since one can write the axial-vector current  $A_\mu$  and the axial-Ward-Takahashi identity that it follows on the lattice [8, 22],  $\Delta_\mu^- A_\mu^a = 2mP^a + 2J_{5q}^a$  with  $\Delta_\mu^-$  the lattice (backward) derivative, the residual mass is naturally defined through matrix elements such as

$$m_{\text{res}} = \frac{\langle 0 | J_{5q}^a | \pi(\vec{p}=0) \rangle}{\langle 0 | P^a | \pi(\vec{p}=0) \rangle}, \quad (2.8)$$

where  $P^a$  is the flavor non-singlet pseudo-scalar density and we chose a zero-momentum pion as the external state. The operator  $J_{5q}^a$  is defined on the (unphysical)  $L_s/2$ -th slice of the 5D space. The calculation of  $m_{\text{res}}$  of this definition requires that the operators  $J_{5q}^a$  and  $P^a$  are sufficiently separated from the source to create the pion state to ensure the dominance of the ground state pion.

An alternative definition that does not refer to any external states may be considered [20]:

$$m_{\text{res}} = \frac{\left\langle \text{Tr} \left[ (\tilde{D}_m^{-1})^\dagger \Delta \tilde{D}_m^{-1} \right] \right\rangle}{\left\langle \text{Tr} \left[ (\tilde{D}_m^{-1})^\dagger \tilde{D}_m^{-1} \right] \right\rangle}. \quad (2.9)$$

The massive quark propagator  $\tilde{D}_m^{-1}$  is given by an inverse of the 4D effective operator up to a contact term

$$\tilde{D}_m^{-1} = \frac{1}{1-m} ((D_{\text{DW}}^{5d}(m))^{-1} - 1), \quad (2.10)$$

which coincides with the surface-to-surface domain-wall propagator. The denominator of (2.9) represents a pseudo-scalar correlator from the origin to arbitrary space-time points summed over, and thus contains the contribution from pion as well as those from excited

states. In the numerator the defect operator  $\Delta$  is inserted to probe the GW violation. It corresponds to the mid-point operator  $J_{5q}^a$  rewritten by the 4D effective field [20].

### C. Meson susceptibilities and chiral condensate

Meson susceptibilities are useful tools to probe the effective restoration of the axial  $U(1)$  symmetry at finite temperature. In particular, we consider the connected pseudoscalar and scalar susceptibilities  $\chi_\pi - \chi_\delta$  that vanishes if the axial symmetry  $U(1)_A$  is restored. It is defined by

$$\chi_\pi - \chi_\delta = \frac{1}{V} \left\langle \int d^4x \pi^a(x) \pi^a(0) - \int d^4x \delta^a(x) \delta^a(0) \right\rangle, \quad (2.11)$$

where  $\pi^a(x) = i\bar{\psi}(x)\gamma_5\tau^a\psi(x)$ ,  $\delta^a(x) = \bar{\psi}(x)\tau^a\psi(x)$  and  $V$  is the space-time volume. In terms of the massive quark propagator  $\tilde{D}_m^{-1}$ , they are written as

$$\chi_\pi = \frac{1}{V} \langle \text{Tr} [(\gamma_5 \tilde{D}_m)^{-2}] \rangle, \quad \chi_\delta = -\frac{1}{V} \langle \text{Tr} [(\tilde{D}_m)^{-2}] \rangle, \quad (2.12)$$

after averaging over the source point. In the continuum theory the difference in (2.11) is written in terms of the Dirac operator eigenvalue spectrum  $\rho(\lambda) = (1/V) \langle \sum_{\lambda'} \delta(\lambda - \lambda') \rangle$  as

$$\chi_\pi - \chi_\delta = \int_0^\infty d\lambda \rho(\lambda) \frac{4m^2}{(m^2 + \lambda^2)^2}, \quad (2.13)$$

as a function of quark mass  $m$ .

Following the similar argument, the chiral condensate  $\langle \bar{\psi}\psi \rangle$  can also be constructed from the propagator,

$$\langle \bar{\psi}\psi \rangle = \frac{1}{V} \langle \text{Tr} [(\tilde{D}_m)^{-1}] \rangle, \quad (2.14)$$

and then in the continuum limit it is written by the spectral function as

$$\langle \bar{\psi}\psi \rangle = \int_0^\infty d\lambda \rho(\lambda) \frac{2m}{m^2 + \lambda^2}, \quad (2.15)$$

which leads to the Banks-Casher relation  $\langle \bar{\psi}\psi \rangle = \pi\rho(0)$  in the thermodynamical limit [23]. Because of the factor  $4m^2/(m^2 + \lambda^2)^2$  in (2.13), the difference  $\chi_\pi - \chi_\delta$  is more sensitive to the lowest end of the spectrum  $\rho(\lambda \approx 0)$ . Having a good control of chiral symmetry is therefore of paramount importance for the difference of the meson susceptibilities.

### III. EIGENMODE DECOMPOSITION WITH THE GINSPARG-WILSON-TYPE FERMIONS

Let us now discuss the decomposition of these observables in terms of the eigenmodes of the Möbius domain-wall Dirac operator at finite  $L_s$ . The operator  $\Delta$  to represent the GW violation is explicitly taken into account. The GW violating terms in the decomposition only depend on the matrix elements of  $\Delta$ , but for the sake of simplicity we define several related quantities during the derivation. In particular, in view of the numerical computation it is easier to define the violation in terms of the matrix elements of  $\gamma_5$ .

#### A. Domain-wall Dirac operator eigenmodes

As a basis for the study of the GW violation, we take the eigenmodes of the hermitian Dirac operator  $H_0 \equiv \gamma_5 D_{\text{DW}}^{4d}(0)$ , or those of the massive operator  $H_m = (1 - m)H_0 + \gamma_5 m$ . The eigenmodes of the hermitian operator are numerically easier to calculate compared to its non-hermitian counterpart. The GW relation (2.6) is rewritten as

$$\{\hat{\gamma}_5, H_0\} = \Delta, \quad (3.1)$$

with  $\hat{\gamma}_5 \equiv \gamma_5 - H_0$ .

The  $n$ -th eigenvalue  $\lambda_n$  and its corresponding eigenmode  $|\psi_n\rangle$  of  $H_m$  satisfy

$$H_m |\psi_n\rangle = \lambda_n |\psi_n\rangle. \quad (3.2)$$

A matrix element of  $\gamma_5$  for these eigenmodes is then written as

$$\langle \psi_n | \gamma_5 | \psi_n \rangle = \frac{\lambda_n^2 + m}{\lambda_n(1 + m)} + g_{nn}, \quad (3.3)$$

where we define the contribution from the GW violating operator  $\Delta$ ,

$$g_{nn} \equiv \frac{(1 - m)^2}{2(1 + m)\lambda_n} \langle \Delta \rangle_{nn}. \quad (3.4)$$

Here and in the following we use a shorthand notation  $\langle \mathcal{O} \rangle_{mn} \equiv \langle \psi_m | \mathcal{O} | \psi_n \rangle$ .

For the chiral condensate  $\Sigma = (1/V) \langle \text{Tr} [\tilde{D}^{-1}] \rangle$ , the decomposition is straightforward using  $\tilde{H}_m^{-1} = \frac{1}{1-m} (H_m^{-1} - \gamma_5)$ , *i.e.*

$$\text{Tr} [\gamma_5 \tilde{H}_m^{-1}] = \frac{1}{1-m} \sum_n \left[ \frac{\langle \gamma_5 \rangle_{nn}}{\lambda_n} - 1 \right] = \frac{m}{1-m^2} \sum_n \frac{1 - \lambda_n^2}{\lambda_n^2} + \frac{1}{1-m} \sum_n \frac{g_{nn}}{\lambda_n}. \quad (3.5)$$

The first term is the physical contribution that survives in the limit of  $L_s \rightarrow \infty$ , while the second term describes the effect of the GW violation.

## B. Decomposition of meson susceptibilities

For the pion susceptibility  $\chi_\pi = (1/V)\langle\text{Tr}[(\gamma_5\tilde{D}_m)^{-2}]\rangle = (1/V)\langle\text{Tr}[\tilde{H}_m^{-2}]\rangle$ , the decomposition is written as

$$\begin{aligned}\text{Tr}[\tilde{H}_m^{-2}] &= \frac{1}{(1-m)^2} \sum_n \langle (H_m^{-1} - \gamma_5)(H_m^{-1} - \gamma_5) \rangle_{nn} \\ &= \frac{1}{1-m^2} \sum_n \frac{1-\lambda_n^2}{\lambda_n^2} - \frac{2}{(1-m)^2} \sum_n \frac{g_{nn}}{\lambda_n}.\end{aligned}\quad (3.6)$$

The first term, that represent the result without any GW relation violation, satisfies  $\text{Tr}[\tilde{H}_m^{-2}] = (1/m)\text{Tr}[\gamma_5\tilde{H}_m^{-1}]$ , which corresponds to the relation  $\chi_\pi = (1/m)\langle\bar{\psi}\psi\rangle$  derived from the axial Ward-Takahashi identity.

The calculation for the  $\delta$  susceptibility  $\chi_\delta = -(1/V)\langle\text{Tr}[\tilde{D}_m^{-2}]\rangle = -(1/V)\langle\text{Tr}[(\gamma_5\tilde{H}_m)^{-2}]\rangle$  requires another set of matrix elements. The first step is

$$\begin{aligned}\text{Tr}[(\gamma_5\tilde{H}_m)^{-2}] &= \frac{1}{(1-m)^2} \sum_n \langle (\gamma_5 H_m^{-1} - 1)(\gamma_5 H_m^{-1} - 1) \rangle_{nn} \\ &= \frac{1}{(1-m)^2} \sum_n \left[ \frac{1}{\lambda_n} \langle \gamma_5 H_m^{-1} \gamma_5 \rangle_{nn} - \frac{2}{\lambda_n} \langle \gamma_5 \rangle_{nn} + 1 \right],\end{aligned}\quad (3.7)$$

where an expression for  $\langle \gamma_5 H_m^{-1} \gamma_5 \rangle_{nn}$  is needed. This can be decomposed into the terms satisfying and violating the GW relation:

$$\langle \gamma_5 H_m^{-1} \gamma_5 \rangle_{nn} = \frac{1}{\lambda_n} \left[ 2 \left( \frac{\lambda_n^2 + m}{\lambda_n(1+m)} \right)^2 - 1 \right] + h_{nn}.\quad (3.8)$$

which defines a new quantity,  $h_{nn}$ , as the defect from the violation of the GW relation. It contains the diagonal elements of  $\langle \Delta \rangle_{nk}$  as well as its off-diagonal components through

$$\begin{aligned}\langle \gamma_5 H_m^{-1} \gamma_5 \rangle_{nn} &= \sum_k \frac{1}{\lambda_k} |\langle \gamma_5 \rangle_{nk}|^2, \\ (1-m)^2 \langle \Delta \rangle_{nk} &= \langle \gamma_5 \rangle_{nk} (1+m)(\lambda_n + \lambda_k) - 2\delta_{nk}(\lambda_n^2 + m).\end{aligned}\quad (3.9)$$

Using these, we obtain

$$\begin{aligned}\text{Tr}[(\gamma_5\tilde{H}_m)^{-2}] &= \frac{1}{(1-m^2)^2} \sum_n \frac{1-\lambda_n^2}{\lambda_n^4} [2m^2 - \lambda_n^2(1+m^2)] \\ &\quad + \frac{1}{(1-m)^2} \sum_n \left[ \frac{h_{nn}}{\lambda_n} - \frac{2g_{nn}}{\lambda_n} \right],\end{aligned}\quad (3.10)$$

where the violation of the GW relation is isolated in the second term.



The difference  $\langle \Delta_{\pi-\delta} \rangle \equiv \chi_\pi - \chi_\delta$  can then be written using

$$\begin{aligned} \Delta_{\pi-\delta} &= \frac{1}{V} (\text{Tr} [\tilde{H}_m^{-2}] + \text{Tr} [(\gamma_5 \tilde{H}_m)^{-2}]) \\ &= \frac{1}{V(1-m^2)^2} \sum_n \frac{2m^2(1-\lambda_n^2)^2}{\lambda_n^4} + \frac{1}{V(1-m)^2} \sum_n \left[ \frac{h_{nn}}{\lambda_n} - \frac{4g_{nn}}{\lambda_n} \right]. \end{aligned} \quad (3.11)$$

For later use, we define  $\Delta_{\pi-\delta}^{\text{GW}}$  and  $\Delta_{\pi-\delta}^{\text{GW}}$  for the first and second term of the right hand side of this equation. Contrary to the individual susceptibilities  $\chi_\pi$  and  $\chi_\delta$ , that have a quadratic ultraviolet divergence, the difference has only a logarithmic divergence in  $\Delta_{\pi-\delta}^{\text{GW}}$ . Notice also that the maximum eigenvalue of the domain-wall effective Dirac operator is one, and the numerator  $(1-\lambda_n^2)^2$  is highly suppressed near the ultraviolet end. Indeed, we can confirm reasonable saturation by summing  $O(10)$  low-lying eigenmodes as discussed in the next section.

### C. Decomposition of residual mass

In order to obtain the eigenvalue decomposition of the residual mass (2.9), we may use

$$\begin{aligned} \text{Tr} [\tilde{H}_m^{-1} \Delta \tilde{H}_m^{-1}] &= \frac{1}{(1-m)^2} \sum_n \left[ \frac{\langle \Delta \rangle_{nn}}{\lambda_n^2} - \frac{2\langle \Delta \gamma_5 \rangle_{nn}}{\lambda_n} + \langle \gamma_5 \Delta \gamma_5 \rangle_{nn} \right] \\ &= \frac{1}{(1-m)^2} \left[ \sum_n \frac{1+\lambda_n^2}{\lambda_n^2} \langle \Delta \rangle_{nn} - \sum_n \frac{2\langle \Delta \gamma_5 \rangle_{nn}}{\lambda_n} \right]. \end{aligned} \quad (3.12)$$

The last equation is exact when we sum over all eigenmodes. The matrix element in the first term  $\langle \Delta \rangle_{nn}$  is proportional to  $g_{nn}$  as in (3.4). The second part, coming from the contact term in the Dirac propagator, includes the off-diagonal elements  $\langle \gamma_5 \rangle_{nk}$  and thus depends also on the off diagonal elements  $\Delta_{nk}$ , like  $h_{nn}$  does. By inserting the complete set of eigenmodes it may also be written as

$$(1-m)^2 \langle \Delta \gamma_5 \rangle_{nn} = (1+m) \sum_k |\langle \gamma_5 \rangle_{kn}|^2 (\lambda_n + \lambda_k) - 2\langle \gamma_5 \rangle_{nn} (\lambda_n^2 + m), \quad (3.13)$$

which is used to evaluate  $\langle \Delta \gamma_5 \rangle_{nn}$  with the low-lying eigenmodes.

The eigenmode decomposition of the residual mass reads

$$m_{\text{res}} = \frac{\left\langle \sum_n \left[ \frac{1+\lambda_n^2}{\lambda_n^2} \langle \Delta \rangle_{nn} - \frac{2}{\lambda_n} \langle \Delta \gamma_5 \rangle_{nn} \right] \right\rangle}{\left\langle \sum_n \left[ \frac{1+\lambda_n^2}{\lambda_n^2} - \frac{2}{\lambda_n} \langle \gamma_5 \rangle_{nn} \right] \right\rangle}. \quad (3.14)$$

The sum on the denominator leads to an ultraviolet divergence, given the asymptotic scaling of the spectral function  $\rho(\lambda) \sim \lambda^3$ . Also, the numerator could diverge unless  $\langle \Delta \rangle_{nn}$  and  $\langle \Delta \gamma_5 \rangle_{nn}$  dump rapidly at high energies. We can still *define* the residual mass with some fixed number of the eigenmodes or at a fixed cutoff on  $\lambda$ , that works as a regularization for this particular quantity. The residual mass thus defined may probe the GW violation at low energies, while the one with all modes is dominated by the contributions of eigenmodes of order of the lattice cutoff.

#### IV. NUMERICAL RESULTS

In this section we show the numerical results obtained on finite temperature lattices, for which the chiral condensate and meson susceptibilities play a crucial role to characterize the property of the phase transition.

##### A. Lattice setup

We perform numerical simulations of two-flavor QCD at finite temperatures near the critical temperature  $T_c \approx 170\text{--}180$  MeV. The temporal extent  $N_t$  is either 8 or 12, and the spatial dimension is  $N_s = 16$  or 32 for  $N_t = 8$  and  $N_s = 32$  for  $N_t = 12$ . We use the tree-level Symanzik improved gauge action and the Möbius domain-wall fermion action. For the Möbius domain-wall fermion, we set  $L_s = 12, 16$  or 24, depending on ensembles. In the following we denote the lattice size in the format  $N_s^3 \times N_t (\times L_s)$ . The three-step stout link-smearing [24] is introduced for the link variables in the domain-wall fermion action, that helps to reduce the residual mass with the modest values of  $L_s$  mentioned above. A wide range of (degenerate) quark masses is taken for some of the ensembles. The residual mass we observe with various definitions is discussed later in the section.

The details of the lattice ensembles used in this analysis are summarized in Table I. We use the standard Hybrid Monte Carlo (HMC) algorithm with multiple integration levels. The simulation code is described in [25]. Unlike the previous work with the overlap fermion formulation [2], we do not introduce the term to prevent the change of global topology [26]. In fact we observe frequent topology tunneling events on these ensembles. These lattices are used in the study of the effective restoration of the axial  $U(1)$  symmetry. Preliminary

$\beta$	$m$	$N_s^3 \times N_t (\times L_s)$	$a$ (fm)	$N_{\text{conf}}$	$N_{\text{ev}}$	$\langle \Delta_{\pi-\delta}^{\text{GW}} \rangle / \langle \Delta_{\pi-\delta}^{(N_{\text{ev}})} \rangle$	$\langle \Delta_{\pi-\delta} \rangle / \langle \Delta_{\pi-\delta}^{(N_{\text{ev}})} \rangle$
4.07	0.01	$16^3 \times 8 (\times 12)$	0.121	239	86	$0.378 \pm 0.026$	$1.0015 \pm 0.0090$
4.10	0.01	$16^3 \times 8 (\times 12)$	0.113	203	86	$0.279 \pm 0.040$	$0.9874 \pm 0.0117$
4.10	0.01	$32^3 \times 8 (\times 12)$	0.113	85	48	$0.302 \pm 0.024$	$1.0074 \pm 0.0057$
4.07	0.001	$16^3 \times 8 (\times 24)$	0.121	210	69	$0.982 \pm 0.002$	$1.0124 \pm 0.0198$
4.07	0.001	$32^3 \times 8 (\times 24)$	0.121	215	25	$0.654 \pm 0.105$	$0.9979 \pm 0.0209$
4.10	0.001	$16^3 \times 8 (\times 24)$	0.113	124	84	$0.983 \pm 0.004$	$0.9937 \pm 0.0162$
4.10	0.005	$32^3 \times 8 (\times 24)$	0.113	98	28	$0.170 \pm 0.023$	$1.0090 \pm 0.0113$
4.10	0.001	$32^3 \times 8 (\times 24)$	0.113	69	36	$0.975 \pm 0.006$	$1.0220 \pm 0.0108$
4.18	0.01	$32^3 \times 8 (\times 12)$	0.096	80	48	$0.616 \pm 0.061$	$1.0969 \pm 0.0279$
4.18	0.01	$32^3 \times 12 (\times 16)$	0.096	54	15	$0.080 \pm 0.006$	$1.0126 \pm 0.0043$
4.22	0.01	$32^3 \times 12 (\times 16)$	0.088	50	38	$0.053 \pm 0.006$	$1.0051 \pm 0.0069$
4.23	0.01	$32^3 \times 12 (\times 16)$	0.086	94	22	$0.038 \pm 0.004$	$1.0020 \pm 0.0056$
4.23	0.005	$32^3 \times 12 (\times 16)$	0.086	176	30	$0.083 \pm 0.009$	$1.0054 \pm 0.0064$
4.23	0.0025	$32^3 \times 12 (\times 16)$	0.086	78	24	$0.162 \pm 0.022$	$1.0028 \pm 0.0119$
4.24	0.01	$32^3 \times 12 (\times 16)$	0.084	326	38	$0.046 \pm 0.003$	$1.0077 \pm 0.0025$
4.24	0.005	$32^3 \times 12 (\times 16)$	0.084	95	33	$0.057 \pm 0.011$	$0.9883 \pm 0.0077$
4.24	0.0025	$32^3 \times 12 (\times 16)$	0.084	111	39	$0.323 \pm 0.080$	$0.9995 \pm 0.0214$
4.30	0.01	$32^3 \times 12 (\times 16)$	0.075	195	38	$0.007 \pm 0.003$	$1.0170 \pm 0.0060$

TABLE I. Lattice ensembles used in this study. The lattices of  $N_t = 8$  ( $=12$ ) are listed in the first (second) block. In the last two columns, the fraction of the GW violating contribution to  $\langle \Delta_{\pi-\delta} \rangle$  as well as of the partial sum up to  $N_{\text{ev}}$  eigenmodes  $\langle \Delta_{\pi-\delta}^{(N_{\text{ev}})} \rangle$  are listed.

results were presented in [27, 28].

On these ensembles we calculate  $N_{\text{ev}}$  lowest-lying eigenvalues and eigenvectors of the hermitian 4D effective Dirac operator  $H_m$ . We use the implicitly restarted Lanczos algorithm to numerically obtain the eigenmodes. For the 4D effective operator, we need an inversion of the Pauli-Villars regulator  $(D_{\text{DW}}^{5d}(1))^{-1}$  for each application of  $H_m$ . The calculation of the eigenmodes is done for configurations separated by at least 20 trajectories of HMC (typically 50).

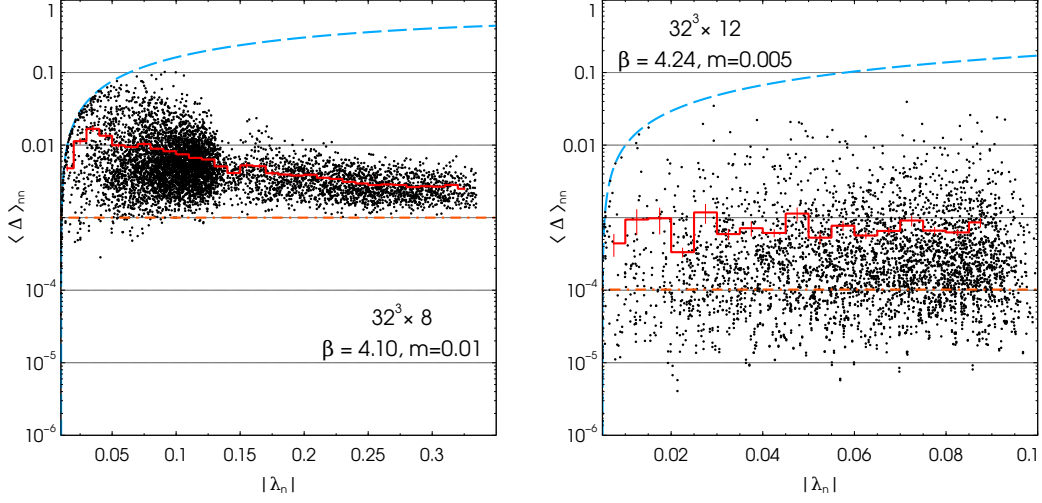


FIG. 1. Scatter plot of  $\langle \Delta \rangle_{nn}$  versus  $\lambda_n$  at  $\beta = 4.10$ ,  $32^3 \times 8$  and  $m = 0.01$  (left), and at  $\beta = 4.24$ ,  $32^3 \times 12$  and  $m = 0.005$  (right). The red thick line shows a binned average in a given range of  $\lambda$ . The blue dashed curve shows the maximal possible violation  $2(\lambda - m)(1 - \lambda)$ , and the orange dash-dot line is the result of the stochastic measurement of the residual mass.

## B. GW violation for individual eigenmodes

Figure 1 shows scatter plots of  $\langle \Delta \rangle_{nn}$  versus  $|\lambda_n|$  for the ensembles of  $\beta = 4.10$ ,  $32^3 \times 8$  ( $\times 12$ ) at  $m = 0.01$  (left) and  $\beta = 4.24$ ,  $32^3 \times 12$  ( $\times 16$ ) at  $m = 0.005$  (right). For individual eigenvalues, the matrix element  $\langle \Delta \rangle_{nn}$  takes the values between roughly  $10^{-3}$  and 0.1 at  $\beta = 4.10$ , and between  $10^{-5}$  and 0.01 at  $\beta = 4.24$  (right). The maximum possible value of  $\langle \Delta \rangle_{nn}$  occurs when  $\langle \gamma_5 \rangle_{nn} = 1$  and is given by  $2(\lambda_n - m)(1 - \lambda)$ , which is shown in the plots by a blue dashed curve.

From Figure 1 we clearly observe that the overall size of  $\langle \Delta \rangle_{nn}$  is made smaller for a finer lattice. The average value calculated in a bin of  $|\lambda_n|$  shows a reduction of an order of magnitude from  $\beta = 4.10$  to 4.24. This is expected because the violation of chiral symmetry should vanish in the continuum limit.

More importantly, the average value for a given range of  $\lambda_n$  gradually decreases for larger  $|\lambda_n|$ . Also shown by a thick dot-dashed line is the corresponding stochastic estimate of the residual mass taking account of all the eigenmodes. The binned average in a given range of  $|\lambda_n|$  shown by red lines indeed shows a tendency approaching the residual mass at large  $\lambda_n$ 's. (The available range of  $\lambda$  is too narrow on the right to see the decrease.) Nearly maximum

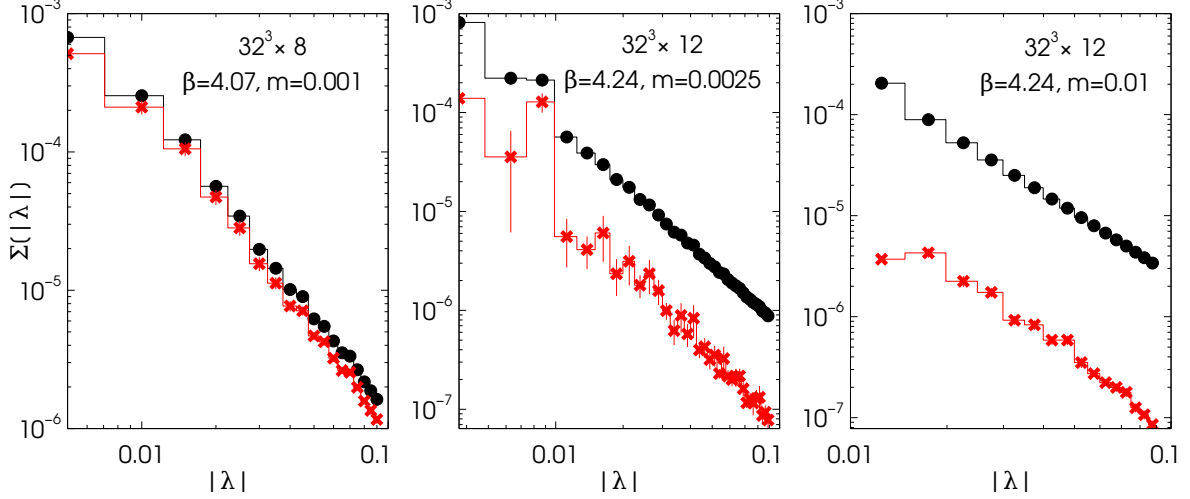


FIG. 2. Contribution of the GW violating term to the chiral condensate averaged in small ranges of  $|\lambda|$ . Black histogram represents the full sum in (3.5) while red crosses show the GW violation term. The data at  $\beta = 4.07$ ,  $32^3 \times 8 (\times 12)$ ,  $m = 0.001$  (left panel),  $\beta = 4.24$ ,  $32^3 \times 12 (\times 16)$ ,  $m = 0.0025$  (middle), and  $\beta = 4.24$ ,  $32^3 \times 12 (\times 16)$ ,  $m = 0.01$  (right panel) are shown.

violation (blue curve) is observed only for near-zero modes.

The  $\langle \Delta \rangle_{nn}$  also appears in the decomposition formula of chiral condensate (3.5). We study the contribution of the GW violating term  $\Sigma^{GW} \equiv (1/V(1-m))\langle \sum_n (g_{nn}/\lambda_n) \rangle$  to the full result by breaking the sum into small ranges of  $|\lambda|$ . In each bin of  $|\lambda|$ , we take an ensemble average and define  $\Sigma[|\lambda|]$  as well as  $\Sigma^{GW}[|\lambda|]$ . Figure 2 shows them as a function of  $|\lambda|$  for comparable temperatures.

The plots demonstrates that the GW violating contribution  $\Sigma^{GW}[|\lambda|]$  to  $\Sigma[|\lambda|]$  is nearly dominating the entire sum on the  $N_t = 8$  lattice (left panel). For most of the low-energy bins, it accounts for more than 50% of the total. For the finer lattice,  $N_t = 12$ , the violating term  $\Sigma^{GW}[|\lambda|]$  becomes 5% or less, when quark mass is large  $m = 0.01$  (right panel). The situation is worse at lower quark mass  $m = 0.0025$  (middle) especially for the lowest-lying bins.

### C. Meson susceptibilities

In this subsection we analyse the meson susceptibilities using the decomposition formulae described in the previous section.

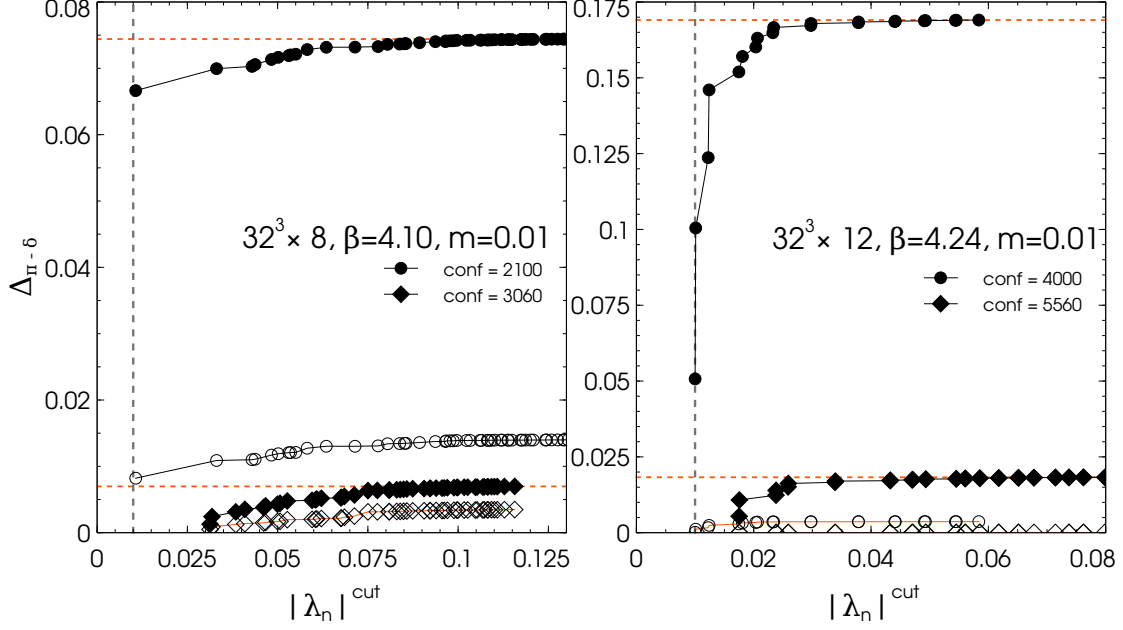


FIG. 3. Accumulated contribution of the low-lying eigenmodes to  $\langle \Delta_{\pi-\delta} \rangle$ . Examples for a couple of gauge configurations are shown for two ensembles:  $\beta = 4.10$ ,  $32^3 \times 8 (\times 12)$ ,  $m = 0.01$  (left) and  $\beta = 4.24$ ,  $32^3 \times 12 (\times 16)$ ,  $m = 0.01$  (right). Circles represent the gauge configurations with exact zero modes  $|\lambda_0| = m$ , while diamonds correspond to those without zero-modes. Empty symbols are the corresponding contribution from the violation terms. The dashed vertical line shows the position of a zero-mode  $|\lambda_0| = m$ . Horizontal lines are the full calculation without the cut, which is obtained by a stochastic method.

First of all, we emphasize that the difference of the meson susceptibilities,  $\langle \Delta_{\pi-\delta} \rangle$ , is highly dominated by the near-zero eigenmodes, because of a strong weight  $1/\lambda_n^4$  for small eigenvalues as can be seen in the decomposition formula (3.11). In particular, the exact zero-mode of  $|\lambda_0| = m$  gives a significant contribution on relatively small lattices, since the first non-zero eigenvalue is well separated by  $\sim 1/\Sigma V$  in the broken phase with the chiral condensate  $\Sigma$ . In the unbroken phase, the non-zero modes are typically even more separated.

A few examples are shown in Figure 3, where the contribution to  $\Delta_{\pi-\delta}$  from low-lying eigenmodes below a cut  $|\lambda_n|^{cut}$  is plotted as a function of  $|\lambda_n|^{cut}$ . We choose a couple of typical gauge configurations with and without exact zero modes. We find that the sum up to  $|\lambda_n|^{cut}$  reaches a plateau at relatively low values of  $|\lambda_n|^{cut}$ ,  $\sim 0.1$  for the lattices of  $\beta = 4.10$ ,  $32^3 \times 8 (\times 12)$ ,  $m = 0.01$  (left), and  $\sim 0.04$  for  $\beta = 4.24$ ,  $32^3 \times 12 (\times 16)$ ,  $m = 0.01$

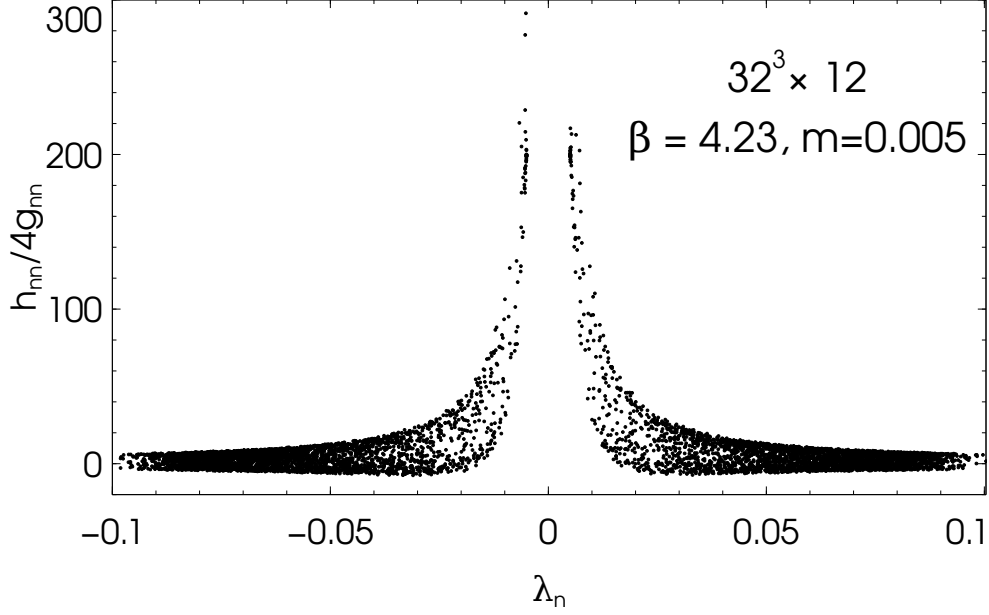


FIG. 4. Ratio  $h_{nn}/4g_{nn}$  for each eigenvalue  $\lambda_n$ . Data at  $\beta = 4.23$ ,  $32^3 \times 12 (\times L_s = 16)$ ,  $m = 0.005$  are shown.

(right).

This plot also shows a significant difference between the gauge configurations with and without the exact zero-modes. The configurations with a zero-mode (circles) give much larger value compared to those without (diamonds). The relative factor is 5–10, depending on the ensembles.

The effect of the GW violating term  $\Delta_{\pi-\delta}^{GW}$  is shown in the same plot by empty symbols. The saturation by low-lying eigenmodes is seen also for this part of  $\Delta_{\pi-\delta}$ .

In  $\Delta_{\pi-\delta}^{GW}$  there are two terms containing  $h_{nn}$  and  $4g_{nn}$ , respectively, as found in (3.11). The latter is proportional to  $\langle \Delta \rangle_{nn}$  while the former needs to be calculated from  $\langle \gamma_5 H_m^{-1} \gamma_5 \rangle_{nn}$ , see (3.8). It turned out that  $h_{nn}$  dominates  $\Delta_{\pi-\delta}^{GW}$  over  $g_{nn}$  as Figure 4 shows. Here, the ratio of the  $h_{nn}$  to  $4g_{nn}$  is plotted for each eigenmode. The enhancement of  $h_{nn}$  near  $|\lambda_n| \simeq 0$  is very steep, and dominates the sum  $\Delta_{\pi-\delta}^{GW}$  by a small number of low-lying modes.

On the two rightmost columns of Table I we summarize the numerical results for  $\langle \Delta_{\pi-\delta}^{GW} \rangle / \langle \Delta_{\pi-\delta}^{(N_{ev})} \rangle$  and  $\langle \Delta_{\pi-\delta} \rangle / \langle \Delta_{\pi-\delta}^{(N_{ev})} \rangle$ . The last column demonstrates the saturation of  $\langle \Delta_{\pi-\delta} \rangle$  with a limited number ( $N_{ev}$ ) of low-lying eigenmodes, which is denoted by  $\langle \Delta_{\pi-\delta}^{(N_{ev})} \rangle$ , for all ensembles we studied. The full calculation is obtained using the stochastic method with 15  $Z_2$  noise vectors. We confirm that this ratio is always consistent with unity.

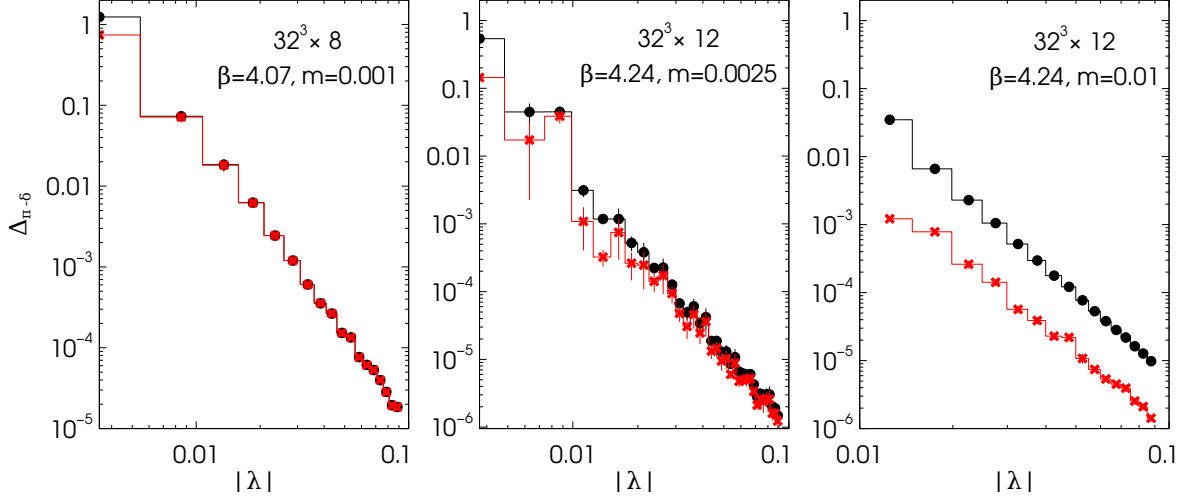


FIG. 5. Eigenmode decomposition of the susceptibility difference  $\Delta_{\pi-\delta}$ . Average in each bin of  $\lambda$  is plotted for full contribution (black circles) and for the contribution from the GW violating term  $\Delta_{\pi-\delta}^{GW}$  (red crosses).

The second last column, on the other hand, shows the fractional size of the GW violating contribution  $\langle \Delta_{\pi-\delta}^{GW} \rangle$  to  $\langle \Delta_{\pi-\delta}^{(N_{ev})} \rangle$ . It shows larger variation between 0 and 1 depending on the ensemble. In the following, we discuss on some remarkable observations.

Figure 5 shows the size of the GW violating contribution  $\Delta_{\pi-\delta}^{GW}$  in the eigenmode decomposition of  $\Delta_{\pi-\delta}$ . For each bin of  $|\lambda|$ , we plot the average of full contribution  $\Delta_{\pi-\delta}$  (black circles) and a partial contribution from the GW violating term  $\Delta_{\pi-\delta}^{GW}$ . We find that on the coarse lattice (left panel:  $\beta = 4.07$ ,  $32^3 \times 8$  ( $\times 24$ ),  $m = 0.001$ ) the GW violating term gives a large fraction, one third of total, at the lowest bin, and it even dominates the signal for other bins. The situation is better on the fine lattice when quark mass is large (right panel:  $\beta = 4.24$ ,  $32^3 \times 12$  ( $\times 16$ ),  $m = 0.01$ ). Namely, the GW violating term is at least one order of magnitude smaller than the total for all the measured bins. Reducing the quark mass (middle panel:  $\beta = 4.24$ ,  $32^3 \times 12$  ( $\times 16$ ),  $m = 0.0025$ ), the GW violating contribution becomes more significant especially for the lowest bins.

Dependence on the lattice spacing is shown in Figure 6, where  $\langle \Delta_{\pi-\delta}^{GW} \rangle / \langle \Delta_{\pi-\delta}^{(N_{ev})} \rangle$  is plotted as a function of  $1/N_t^2$ . For the same (or similar) temperature, it effectively shows the dependence on the lattice spacing squared  $a^2$ . The plot clearly shows that the GW violating contribution  $\langle \Delta_{\pi-\delta}^{GW} \rangle$  is substantial for the lattices of  $N_t = 8$ . It can be as large as 30% or even 60% of the total, which is clearly not in the region where the usual  $O(a^2)$  scaling toward the



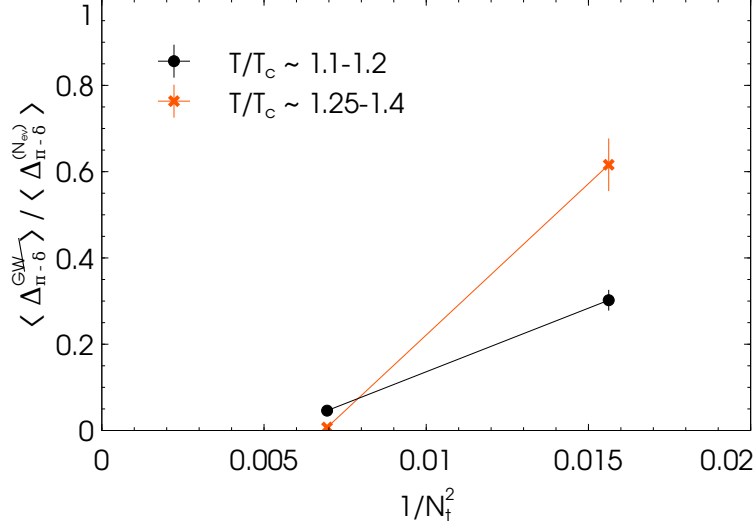


FIG. 6. Fractional contribution of the GW violating term to  $\langle \Delta_{\pi-\delta} \rangle$ , *i.e.*  $\langle \Delta_{\pi-\delta}^{GW} \rangle / \langle \Delta_{\pi-\delta}^{(N_{ev})} \rangle$ , as a function of  $1/N_t^2$ . For a constant temperature, or  $T/T_c$ , it represents the dependence on  $a^2$ . We plot the lattice data corresponding to  $T/T_c \simeq 1.1-1.2$  (circles) and to  $1.25-1.4$  (crosses). The quark mass is  $m = 0.01$  for all the data points which are respectively  $\beta = 4.10, 4.24$  and  $\beta = 4.18, 4.30$ .

continuum limit is applied. Such artifact due to finite lattice spacing is significantly reduced at  $N_t = 12$ .

Figure 7 shows the dependence of  $\langle \Delta_{\pi-\delta}^{GW} \rangle / \langle \Delta_{\pi-\delta}^{(N_{ev})} \rangle$  on the quark mass  $m$ . The data are those of  $N_t = 12$ , for which the lattice artifact is relatively small. We observe that the GW violating term is strongly enhanced for small quark masses.

By varying  $\beta$  at a fixed  $N_t$  ( $=12$ ) we may study the dependence of the GW violation on temperature. From  $\beta = 4.18$  to  $4.24$  at  $N_t = 12$ , the system goes across the critical temperature. Figure 8 shows how  $\langle \Delta_{\pi-\delta}^{GW} \rangle / \langle \Delta_{\pi-\delta}^{(N_{ev})} \rangle$  depends on  $\beta$ . We clearly see an increase of the violating term towards the lower  $\beta$  values, which can be understood partly as an effect of larger lattice spacing. It could be enhanced further by the accumulation of low-lying modes in the chirally broken phase.

#### D. Residual mass

In this subsection we numerically study the eigenmode decomposition of the residual mass, starting from the expression (3.14).

We first show that the second term on the numerator of (3.14) has only subdominant

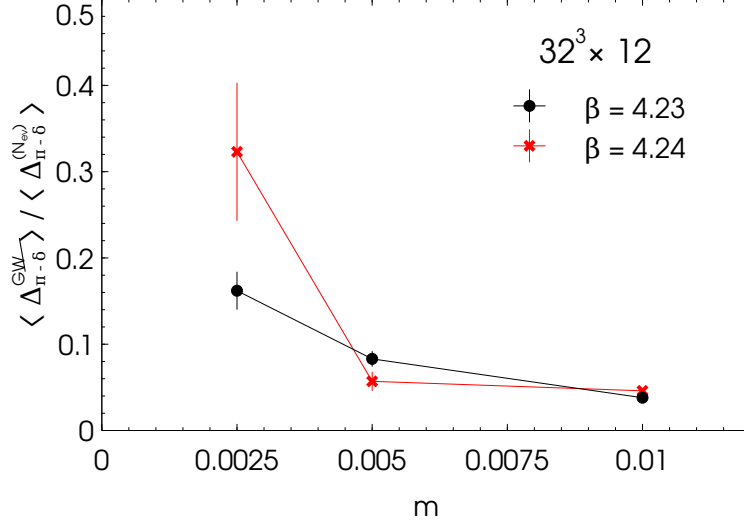


FIG. 7. Fractional contribution of the GW violating term to  $\langle \Delta_{\pi-\delta} \rangle$ , *i.e.*  $\langle \Delta_{\pi-\delta}^{\text{GW}} \rangle / \langle \Delta_{\pi-\delta}^{(N_{\text{ev}})} \rangle$ , as a function of  $m$ . The lattice data at  $\beta = 4.23$ ,  $32^3 \times 12 (\times 16)$  (circles) and  $\beta = 4.24$ ,  $32^3 \times 12 (\times 16)$  (crosses) are plotted.

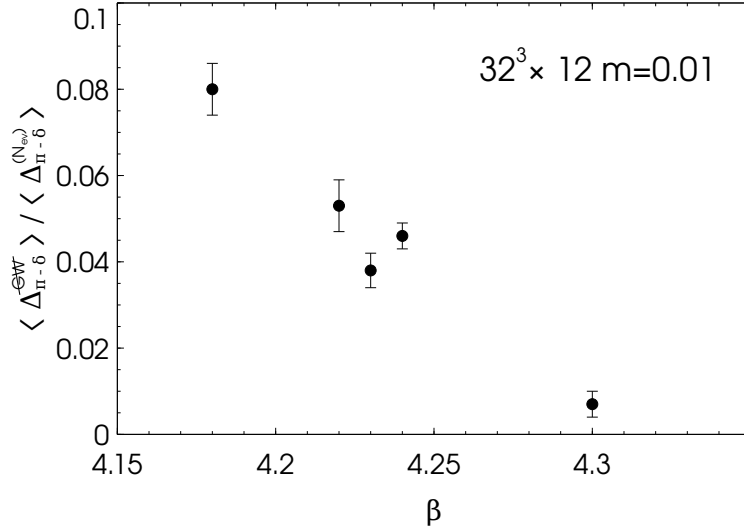


FIG. 8. Fractional contribution of the GW violating term to  $\langle \Delta_{\pi-\delta} \rangle$ , *i.e.*  $\langle \Delta_{\pi-\delta}^{\text{GW}} \rangle / \langle \Delta_{\pi-\delta}^{(N_{\text{ev}})} \rangle$ , as a function of  $\beta$ . At a fixed  $N_t$ , this effectively represents the dependence on temperature.

contributions. In Figure 9, we plot  $|(1 + \lambda_n^2) \langle \Delta \rangle_{nn} / (2\lambda_n \langle \Delta \gamma_5 \rangle_{nn})|$  for each eigenmode as a function of  $|\lambda_n|$ . This corresponds to a ratio of the first term to the second in the numerator of (3.14). We find that the first term is typically 10–100 larger than the second term especially for the low-lying modes. It implies that we can safely neglect the term of  $\langle \Delta \gamma_5 \rangle_{nn}$  in the evaluation of  $m_{\text{res}}$ .

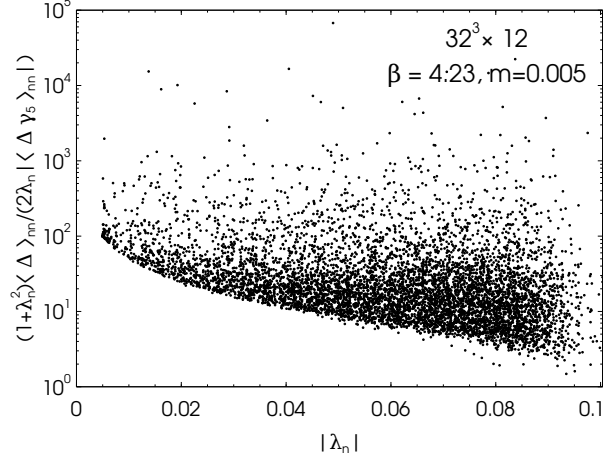


FIG. 9. Ratio of the first term on the numerator in the eigenmode decomposition of  $m_{\text{res}}$  (3.14) to the second term. Explicitly, it is written as  $|(1 + \lambda_n^2)\langle\Delta\rangle_{nn}/(2\lambda_n\langle\Delta\gamma_5\rangle_{nn})|$ . The plot shows the value for each eigenmode as a function of  $|\lambda_n|$ . Data at  $\beta = 4.23$ ,  $32^3 \times 12 (\times 16)$ ,  $m = 0.005$  are plotted.

The same observation applies also for the denominator, *i.e.* the contribution of the second term  $2\langle\gamma_5\rangle_{nn}/\lambda_n$  is negligible compared to the first  $(1 + \lambda_n^2)/\lambda_n^2$ . The residual mass is then precisely approximated by a weighted average of  $\langle\Delta\rangle_{nn}$  of the form

$$m_{\text{res}} \simeq \frac{\sum_n \frac{1 + \lambda_n^2}{\lambda_n^2} \langle\Delta\rangle_{nn}}{\sum_n \frac{1 + \lambda_n^2}{\lambda_n^2}}. \quad (4.1)$$

We can therefore gain a rough idea of the residual mass by inspecting  $\langle\Delta\rangle_{nn}$ . From the plots in Figure 1 we find that  $\langle\Delta\rangle_{nn}$  is approximately constant in the lowest part of the spectrum. On the other hand, we can calculate  $m_{\text{res}}$  using a stochastic method, the result of which is shown by a dot-dashed line in the plots of Figure 1. We find that the contribution from the individual low-lying eigenmodes  $\langle\Delta\rangle_{nn}$  is typically one order of magnitude larger than the weighted average  $m_{\text{res}}$ , while the average of  $\langle\Delta\rangle_{nn}$  in a bin of  $|\lambda_n|$  tends to decrease towards the stochastic estimates for larger  $|\lambda_n|$ . It implies that the GW violating effect is enhanced in the low-lying modes.

We estimated the residual mass in the low-mode region by applying an arbitrary upper-cut, that we chose  $\lambda_{\text{cut}} = 0.08$ , to the eigenvalue sums in the numerator and in the denominator. The results are listed in Table II. They confirm that in this region of the spectrum

$\beta$	$m$	$N_s^3 \times N_t (\times L_s)$	$m_{\text{res}} (\lambda_n < 0.08)$	$m_{\text{res}} (\text{stochastic})$
4.10	0.01	$32^3 \times 8 (\times 12)$	0.0065(5)	0.0010(2)
4.10	0.005	$32^3 \times 8 (\times 24)$	0.0030(3)	0.00053(4)
4.18	0.01	$32^3 \times 12 (\times 16)$	0.0010(1)	0.00022(2)
4.23	0.01	$32^3 \times 12 (\times 16)$	0.00047(5)	0.00010(1)
4.24	0.01	$32^3 \times 12 (\times 16)$	0.00068(12)	0.00009(1)
4.23	0.005	$32^3 \times 12 (\times 16)$	0.00063(6)	0.00012(2)
4.24	0.005	$32^3 \times 12 (\times 16)$	0.00048(7)	0.00010(2)
4.23	0.0025	$32^3 \times 12 (\times 16)$	0.00066(7)	0.00016(4)
4.24	0.0025	$32^3 \times 12 (\times 16)$	0.00107(17)	0.00013(3)

TABLE II. Residual mass calculated using the lowest part of the spectrum ( $\lambda_n < 0.08$ ) compared with full result obtained with a stochastic measurement.

the effective residual mass is significantly larger, as expected from the observation of  $\langle \Delta \rangle_{nn}$ .

The residual mass as obtained with (3.14) is dominated by the ultraviolet part of the eigenmodes because of the increasing number of the eigenmodes  $\sim \lambda^3$ , even though the weight factor  $\frac{1+\lambda_n^2}{\lambda_n^2}$  would favor the infrared region. This is qualitatively in agreement with the fact that the residual mass calculated with the pion external state (2.8) is significantly larger than the full summation of the space-time points (2.9). (See a discussion in [29] for more details).

## V. SUMMARY

The remnant violation of the GW relation is a potential source of substantial systematic error for some physical quantities, for which the low-lying eigenmode give a significant (or even dominant) contribution. In this work we have shown how to identify the effect of the violation in the meson susceptibilities, chiral condensate and the residual mass by decomposing their matrix elements in the Dirac eigenmode basis. We obtained exact equations that account for the violation terms and allow their quantitative estimate. All the violation terms can be described in terms of the matrix elements of  $\gamma_5$  in the eigenmode basis.

Numerical calculations show that the difference of susceptibilities  $\Delta_{\pi-\delta}$  can be strongly

affected by the violations coming from the lowest part of the spectrum on coarse lattices. The signal for Möbius domain-wall fermions at lattice spacings  $> 0.1$  fm is dominated by lattice artifacts making the naive calculation unreliable. At finer lattices,  $\sim 0.08$  fm, the effect is reduced dramatically to a more manageable level, 10–20%. The mass dependence, showing an increase of the effect in the  $m \rightarrow 0$  limit, confirms that the lowest-eigenmode region is critical and finer lattices are necessary for a proper chiral limit using the Möbius domain-wall fermions.

The analogous expansion of the residual mass shows another example that the lowest part of the spectrum has larger violations to the Ginsparg-Wilson relation. The estimate of  $m_{\text{res}}$  in this spectral region shows that the naive estimate is about one order of magnitude smaller, potentially underestimating the GW-violating contributions. The effect of the remnant chiral symmetry violation needs to be estimated for individual quantities of interest, and the definition of  $m_{\text{res}}$  constructed from the low-lying modes is more adequate for the quantities dominated by the lowmodes.

## ACKNOWLEDGMENTS

Numerical simulations are performed on IBM System Blue Gene Solution at High Energy Accelerator Research Organization (KEK) under a support for is Large Scale Simulation Program (No. 14/15-10). This work is supported in part by the Grant-in-Aid of the Ministry of Education (No. 25800147, 26247043, 15K05065) and by MEXT SPIRE and JICFuS.

- 
- [1] E. Shintani, S. Aoki, H. Fukaya, S. Hashimoto, T. Kaneko, H. Matsufuru, T. Onogi, and N. Yamada (JLQCD), Phys. Rev. Lett. **101**, 242001 (2008), arXiv:0806.4222 [hep-lat].
  - [2] G. Cossu, S. Aoki, H. Fukaya, S. Hashimoto, T. Kaneko, H. Matsufuru, and J.-I. Noaki, Phys. Rev. **D87**, 114514 (2013), [Erratum: Phys. Rev.D88,no.1,019901(2013)], arXiv:1304.6145 [hep-lat].
  - [3] M. I. Buchoff et al., Phys. Rev. **D89**, 054514 (2014), arXiv:1309.4149 [hep-lat].
  - [4] T.-W. Chiu, W.-P. Chen, Y.-C. Chen, H.-Y. Chou, and T.-H. Hsieh (TWQCD), PoS **LATTICE2013**, 165 (2014), arXiv:1311.6220 [hep-lat].
  - [5] B. B. Brandt, A. Francis, H. B. Meyer, O. Philipsen, and H. Wittig, PoS **LATTICE2013**, 162 (2014), arXiv:1310.8326 [hep-lat].
  - [6] D. B. Kaplan, Phys. Lett. **B288**, 342 (1992), arXiv:hep-lat/9206013 [hep-lat].
  - [7] Y. Shamir, Nucl. Phys. **B406**, 90 (1993), arXiv:hep-lat/9303005 [hep-lat].
  - [8] V. Furman and Y. Shamir, Nucl. Phys. **B439**, 54 (1995), arXiv:hep-lat/9405004 [hep-lat].
  - [9] H. Neuberger, Phys. Lett. **B417**, 141 (1998), arXiv:hep-lat/9707022 [hep-lat].
  - [10] H. Neuberger, Phys. Rev. Lett. **81**, 4060 (1998), arXiv:hep-lat/9806025 [hep-lat].
  - [11] H. B. Nielsen and M. Ninomiya, Phys. Lett. **B105**, 219 (1981).
  - [12] P. H. Ginsparg and K. G. Wilson, Phys. Rev. **D25**, 2649 (1982).
  - [13] M. Luscher, Phys. Lett. **B428**, 342 (1998), arXiv:hep-lat/9802011 [hep-lat].
  - [14] S. Aoki et al. (JLQCD), Phys. Rev. **D78**, 014508 (2008), arXiv:0803.3197 [hep-lat].
  - [15] S. Borsanyi, Y. Delgado, S. Durr, Z. Fodor, S. D. Katz, S. Krieg, T. Lippert, D. Nogradi, and K. K. Szabo, Phys. Lett. **B713**, 342 (2012), arXiv:1204.4089 [hep-lat].
  - [16] R. Narayanan and H. Neuberger, Phys. Lett. **B302**, 62 (1993), arXiv:hep-lat/9212019 [hep-lat].
  - [17] R. Narayanan and H. Neuberger, Phys. Rev. Lett. **71**, 3251 (1993), arXiv:hep-lat/9308011 [hep-lat].
  - [18] R. Narayanan and H. Neuberger, Nucl. Phys. **B412**, 574 (1994), arXiv:hep-lat/9307006 [hep-lat].
  - [19] Y. Kikukawa and T. Noguchi, (1999), 10.1016/S0920-5632(00)91758-4, arXiv:hep-lat/9902022 [hep-lat].
  - [20] R. C. Brower, H. Neff, and K. Orginos, (2012), arXiv:1206.5214 [hep-lat].

- [21] A. Borici, Lattice field theory. Proceedings, 17th International Symposium, Lattice'99, Pisa, Italy, June 29-July 3, 1999, Nucl. Phys. Proc. Suppl. **83**, 771 (2000), arXiv:hep-lat/9909057 [hep-lat].
- [22] P. A. Boyle (UKQCD), Proceedings, 32nd International Symposium on Lattice Field Theory (Lattice 2014), PoS LATTICE2014, 087 (2015).
- [23] T. Banks and A. Casher, Nucl. Phys. **B169**, 103 (1980).
- [24] C. Morningstar and M. J. Peardon, Phys. Rev. **D69**, 054501 (2004), arXiv:hep-lat/0311018 [hep-lat].
- [25] G. Cossu, J. Noaki, S. Hashimoto, T. Kaneko, H. Fukaya, et al., PoS **LATTICE2013**, 482 (2013), arXiv:1311.0084 [hep-lat].
- [26] H. Fukaya, S. Hashimoto, K.-I. Ishikawa, T. Kaneko, H. Matsufuru, T. Onogi, and N. Yamada (JLQCD), Phys. Rev. **D74**, 094505 (2006), arXiv:hep-lat/0607020 [hep-lat].
- [27] G. Cossu, H. Fukaya, S. Hashimoto, T. Kaneko, J.-i. Noaki, and A. Tomiya (JLQCD), Proceedings, 32nd International Symposium on Lattice Field Theory (Lattice 2014), PoS **LATTICE2014**, 210 (2015), arXiv:1412.5703 [hep-lat].
- [28] A. Tomiya, G. Cossu, H. Fukaya, S. Hashimoto, and J. Noaki, Proceedings, 32nd International Symposium on Lattice Field Theory (Lattice 2014), PoS **LATTICE2014**, 211 (2015), arXiv:1412.7306 [hep-lat].
- [29] A. Jüttner, L. Del Debbio, N. Garron, A. Khamseh, M. Marinkovic, F. Sanfilippo, J. T. Tsang, and P. A. Boyle, Proceedings, 32nd International Symposium on Lattice Field Theory (Lattice 2014), PoS **LATTICE2014**, 380 (2015), arXiv:1502.00845 [hep-lat].